ACSNANO
www.acsnano.org
ARTICLE

Superwettable Microchips as a Platform toward Microgravity Biosensing

Tailin Xu,[†] Wanxin Shi,[†] Jinrong Huang,[†] Yongchao Song,[†] Feilong Zhang,[‡] Li-Ping Xu,*[,†] Xueji Zhang,*[,†] and Shutao Wang*[,‡]

[†]Research Center for Bioengineering and Sensing Technology, School of Chemistry and Biological Engineering, University of Science and Technology Beijing, Beijing 100083, P. R. China

[‡]CAS Key Laboratory of Bio-inspired Materials and Interfacial Science, CAS Center for Excellence in Nanoscience, Technical Institute of Physics and Chemistry, Chinese Academy of Sciences, Beijing 100190, P. R. China

Supporting Information

ABSTRACT: **The construction of the Space Station provides a spaceflight laboratory, which enables us to accomplish tremendous short- and long-duration research such as astronomy, physics, material sciences, and life sciences in a microgravity environment. Continuous innovation and development of spaceflight laboratory prompted us to develop a facile detection approach to meet stringent requirements in a microgravity environment that traditional experimental approaches cannot reach. Here we introduce superhydrophilic microwells onto superhydrophobic substrates that are capable of capturing and transferring microdroplets, demonstrating a proof-of-concept study of a biosensing platform toward microgravity application. The capability of manipulating microdroplets originates from the capillary force of the nanoscale dendritic coating in superhydrophilic microwells. Based on theoretical modeling, capillary forces of the superhydrophilic microwells can dominate the behavior of microdroplets against the gravity. Direct naked-eye observation monitoring of daily physiological markers, such as glucose, calcium, and protein can be achieved by colorimetric tests without the requirement of heavy optical or electrical equipment, which greatly reduced the weight, and will bring a promising clue for biodetection in microgravity environments.**

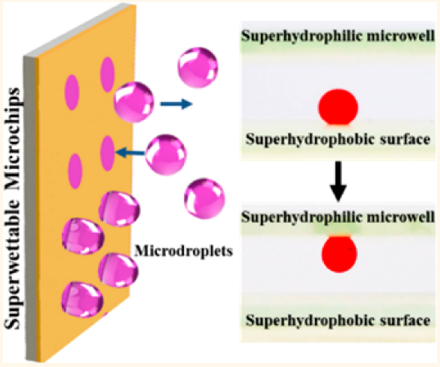

KEYWORDS: *superhydrophilic, superhydrophobic, microgravity, biosensing, colorimetric biosensor, superwettable microchips*

The research in the Space Station spaceflight laboratory has already led to major advances in science and technology, impacting diverse areas such as human health, animal, plant, and microbial research and materials science.[1,2] However, the astronauts dedicated to the research in Space Station may suffer from many serious adverse physiological changes, such as bone fracture, muscle atrophy, and gene or protein expression induced medical problems during the spaceflight.[3−6] For example, clinical studies have confirmed that those astronauts experienced excessive metabolism of bone calcium with a minimum 5% loss to 10% or greater loss in at least one skeletal site after a long-duration spaceflight.[7] Current diagnostic technologies for the detection of physiological markers in microgravity always require skilled technicians or sophisticated instrumentation, and weightlessness or zero gravity results in microdroplets floating everywhere, which makes the contact detection process much more complicated. So, the challenge remains to develop an alternative to meet the high standards of microgravity conditions.

A growing number of microdroplet-based biosensors are reported for diagnostic applications including biomolecular detections, plasmonic immunoassays, cell behavior investigation, *etc.*[8−12] These microdroplets provide a miniature "vessel" for bioanalysis, which offers several benefits including portability and facile and high throughput.[13−16] Recently, superwettable microchips with superhydrophobic−superhydrophilic patterns exhibit excellent ability of patterning microdroplets[17−21] and have a profound impact upon diverse applications such as ultratrace detection of DNA[22] and cell microarray.[23−27] Importantly, superwettable materials[28−36] have proved to control the motion of liquid droplets, for example, their directional motion on anisotropic wettable surface[37−39] and transferring between two surfaces by using a superhydrophobic surface with high adhesion.[40,41] These studies provide an opportunity to manipulate microdroplets toward biosensing in microgravity condition.

Received: October 12, 2016
Accepted: December 19, 2016
Published: December 19, 2016

DOI: 10.1021/acsnano.6b06896
ACS Nano 2017, 11, 621−626

Herein, we introduced a superhydrophilic−superhydrophobic microchip with the capability of capturing microdroplets as a platform to perform detection of routine biomarkers toward microgravity biosensing. On the superwettable microchip, the high droplet-capturing ability of superhydrophilic microwells can capture water droplets, while low adhesion of superhydrophobic background can limit the motion of the droplet. The high droplet-capturing ability of superhydrophilic microwells originates from a capillary force of their nanodendritic silica coating and results in the detection processes easily at weightlessness or zero gravity conditions. We successfully employed this microchip in a proof-of-concept detection of routine physiological markers (such as glucose, calcium, and protein) regardless of the gravity. Contrast to the microfluidic related system,[42−44] which requires additional equipment (pump, microscope, and electronic control system) that brings a heavy burden during the spaceflight, and bubbles easily appear and exit in such a closed container under a microgravity environment. Such a microchip with the advantages of simple, easy to operate, low-weight, robustness, and easy read-out technology that meets the high standards of space research will hold great potential in monitoring the health conditions of humans inside the space station.

RESULTS AND DISCUSSION

Figure 1a illustrates the simple experimental procedures of fabrication of superhydrophilic microwells on the superhydrophobic nanodendritic silica coating. In brief, a superhydrophobic nanodendritic silica coating with a contact angle of 157.6° ± 2.5° (Figure 1b, left) was first fabricated as previously reported.[45−47] This simple approach employs a candle soot as the template and provides a robust way to develop a superwettable coating. The nanodendritic superhydrophobic coating candle soot exhibits a dendritic-like network, consisting of physically connected and approximately spherical soot particles with a diameter ranging from 19 to 43 nm, as demonstrated in Figure 1d. Then, superhydrophilic microwells on an octadecytrichlorosilane (OTS)-modified nanodendritic coating was fabricated *via* UV irradiation through photomask. After 40 min of irradiation, the OTS in the exposed area was photodecomposed and formed superhydrophilic microwells with a contact angle of around 0° (Figure 1b, right). The prepared superwettable microchips also show great robustness (without malicious mechanical damage and long-term strong ultraviolet irradiation) due to the stability of physical and chemical properties of the superhydrophobic SiO_2 layer. Allura-red-labeled water droplets on the as-prepared substrate present two diametrically opposed appearances. On the OTS-modified surface, water droplet was almost spherical and indicates its superhydrophobicity (Figure 1c, left top). In contrast, water droplets were flattened in microwells, revealing its superhydrophilicity (enlarged view in Figure 1c). Thus, we prepared the superhydrophilic−superhydrophobic microchip toward microgravity biosensing.

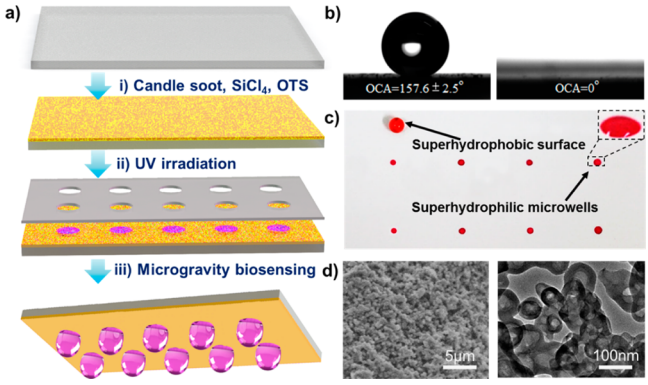

Figure 1. Fabrication and characterizations of nanodendritic superwettable microchips. (a) Schematic illustration of fabrication processes of nanodendritic superwettable microchips following by coating candle soot, OTS modification, and photomask-assisted UV irradiation, and their potential application toward microgravity biosensing. (b) Water contact angle of the before OTS-modified nanodendritic silica coating (left) and after UV-irradiation (right). (c) Allura-red-labeled water microdroplets on the surfaces of superhydrophobic OTS-nanodendritic silica coating and on superhydrophilic microwells. (d) SEM and TEM images of the nanodendritic silica coating.

The superwettable microchips showed the unique ability of capturing microdroplets. Their capture capacity was investigated by monitoring the behaviors of microdroplets on superwettable microchips, as illustrated in Figure 2a. In brief, 5 μL water droplet dyed with allura red was added onto the prepared superhydrophobic substrate (Figure 2a left). When microchip with the microwell diameter of 0.5 mm approached and attached to the microdroplet, the microdroplet was

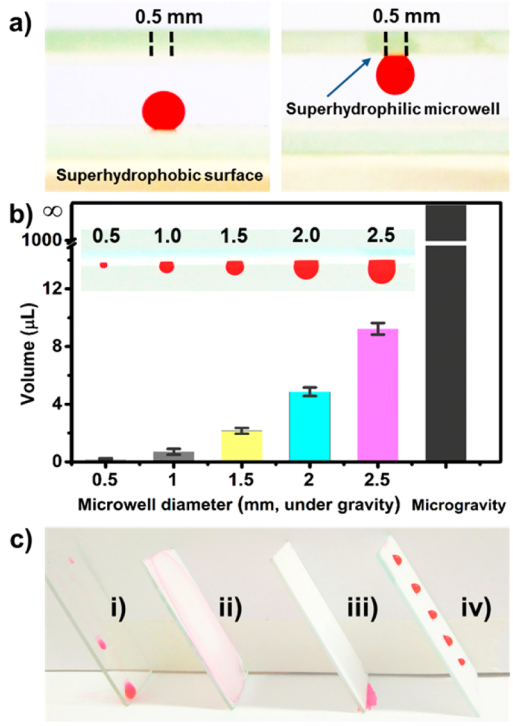

Figure 2. Investigation of the microdroplets behavior on superhydrophilic−superhydrophobic microwells. (a) Before (left) and after (right) superhydrophilic microwell (diameter: 0.5 mm) capture of microdroplets on the superhydrophobic surface. (b) Capture of microdroplets from allura-red-dyed water with different diameters of microwells (0.5, 1.0, 1.5, 2.0, and 2.5 mm). (c) Contrast of the microdroplets behavior (15 μL) on four different substrates: (i) bare glass surface, (ii) superhydrophilic surface, (iii) superhydrophobic surface, and (iv) superwettable microchips; microdroplets array formed on superwettable microchips confirmed its unique ability of capturing and holding in superhydrophilic microwells.

DOI: 10.1021/acsnano.6b06896
ACS Nano 2017, 11, 621−626

immediately captured by the upper superwettable microchip (Figure 2a right), indicating the capturing ability of the superhydrophilic microwell. The as-prepared microchip with captured microdroplets can also hold the microdroplets easily even when vertically flipped. As demonstrated in Figure S1, patterned microdroplets displayed elongated ellipsoids when the substrate was reversed to 0°, 135°, and 180° without dropping down from the substrate, suggesting their holding capability of water microdroplets.

The volume of captured microdroplet depends on the diameters of superhydrophilic microwells. Figure 2b illustrates the capture ability of different volumes of microdroplets by using different diameters of superhydrophilic microwells. Microwells were fabricated *via* UV irradiation through photomasks with the holes varied from 0.5, 1.0, 1.5, 2.0 to 2.5 mm. The whole glass was immersed in allura-red-dyed water for 1 s and then pull out. Microdroplets were captured and patterned on the microwells against the gravity and displayed an increase in volume from 0.2, 0.7, 2.15, 4.86 to 9.23 μL along with the size of the microwells, as demonstrated in Figure 2b. Visual comparison of the capture ability of two microwells (2 mm *vs* 2 mm, 2 mm *vs* 0.5 mm) is demonstrated in Figure S2. Gradually taking the upper microchips away from the lower ones resulted in stretching of the microdroplets, and a thin neck next to the smaller side was formed (Figure S2b, step 3). Such dependence reflects the relationship between the capture volumes and the diameters of superhydrophilic microwells. Even under gravity, the superwettable microchip can capture microdroplets from the solution, implying the possibility of capturing an infinity volume of water droplets under microgravity conditions. In addition, we also compared our superwettable microchips with three other glass substrates, including bare glass surface, superhydrophilic surface, and superhydrophobic surface, to further investigate its capture capability. These four substrates were placed 60° between the horizontal plane, then a 15 μL allura-red-dyed water droplet was dropwised from the top. As demonstrated in Figure 2c, water droplets flowed down from the bare glass surface, the superhydrophilic surface was fully wetted by water droplets, and microdroplets slipped off from superhydrophobic surface. In contrast, array microdroplets forming on superwettable microchips further confirmed their unique ability of capturing and holding in superhydrophilic microwells.

We attempted to explain the unique capture phenomena of superwettable microchips by using a simplified capillary model between liquid and porous solid surfaces. Compared to flat glass, our superhydrophilic microwells with porous nanodendritic structures exhibit a larger adhesive force to water microdroplets. Here, a thermodynamic parameter, work of adhesion (W_{sl}), was introduced to evaluate the characteristic of the liquid/porous solid pair, which is related to the surface tension of the liquid, the wicking constant of the wetting liquid, and the surface area of nanodendritic structure. In our experiment, the surface area of porous nanodendritic structure was related to the size and distribution of nanopore, which can be modeled as an array of straight nonconnected parallel circular cylinders with different diameters passing through the nanodendritic coating (see Figure 3), thus the total capillary force is the sum of each individual nanopore.[48] As a result, the absolute value of work of adhesion used to separate the liquid from the pore wall can be considered as follows:[49]

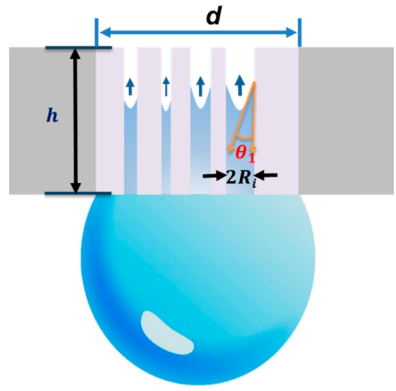

Figure 3. Schematic of the microdroplet behavior on the nanoporous substrate, where h is the thickness of the nanodendritic coating, R_i is the radius of the i^{th} of nanopore, d is the diameter of microwells, and θ is the equilibrium contact angle of water on the surface of the nanodendritic coating.

$$W_{sl} = \sum_{i=1}^{n=N_p} 2\sigma(1 + \cos\theta)\pi R_i h \tag{1}$$

where σ is the surface tension of the sample solution (in our case is water), θ is the equilibrium contact angle of water with the surface of the nanodendritic, R_i is the radius of i^{th} nanopore, and h is the thickness of the nanodendritic coating, which can be controlled by moving the substrate back-and-forth on a steady burning candle and also can be visualized by SEM images. Thus, the model of an array on nanodendritic coating requires knowing the probability density function $U(R)$ and the number of nanopores (N_p). For given diameter of microwells (d), the number of nanopores can be calculated as follows:

$$N_p = \frac{1/4\varepsilon\pi d^2}{\int \pi R^2 U(R) dR} \tag{2}$$

where ε is the porosity of the samples, $1/4\varepsilon\pi d^2$ means the sum of cross-sectional area of the given microwell (d). The distribution function of the nanopores can be expressed by normal Gaussian distribution: Distribution function of pore radius $U(R)$, is a pore with a given radius R within a range of dR.

$$U(R) = \frac{1}{\sqrt{2\pi\sigma_R{}^2}} \exp\left(\frac{-(R-\mu_R)^2}{2\sigma_R{}^2}\right) \tag{3}$$

where μ_R is the mean of the pore radius of nanodendritic coating, and σ_R is the standard deviation of the nanopores radius; both of them can be obtained from the SEM images.

Based on this model, the work of adhesion of a given liquid to the porous material can be calculated and allows determining the adhesion between liquids and porous solids. We can derive that the increase of the thickness of nanodendritic coating (h), the diameter of microwells (d), and surface tension (σ) equilibrium contact angle (θ) or reduction of the radius of nanopore (R) could increase the work of adhesion and result in increasing capture capability. However, in our case, σ, h, R, and θ are situations or a state of affairs that we do not change, and as a result, capture capability can be modified by increasing the diameter of microwells. The theoretical modeling also meets the competitive capture of the microdroplet experiment, as demonstrated in Figure S2.

DOI: 10.1021/acsnano.6b06896
ACS Nano 2017, 11, 621−626

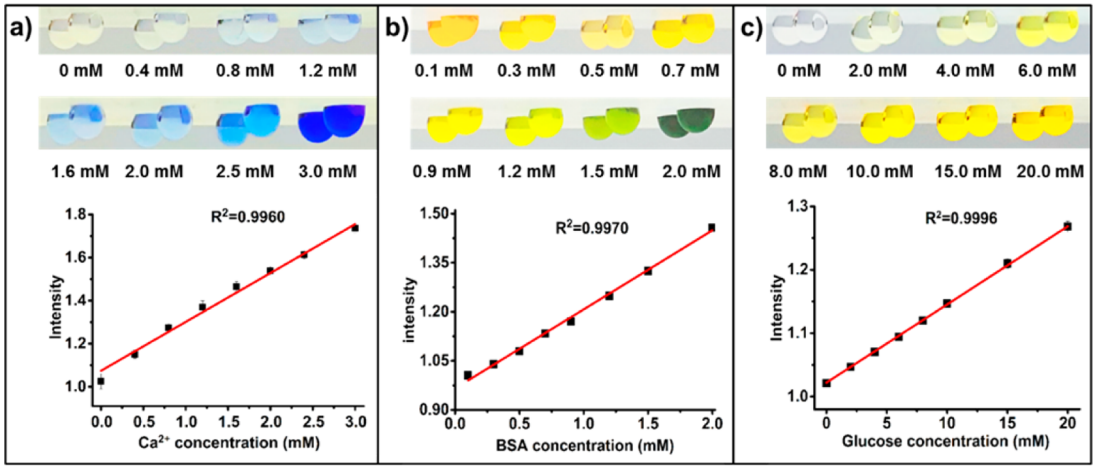

Figure 4. Application of superwettable microchips in quantitatively colorimetrical detection of routine physiological markers. Colorimetrical calibration curve of (a) calcium from 0 mM to 3.0 mM, (b) protein from 0 mM to 2.0 mM, and (c) glucose from 0 mM to 20.0 mM, with correlation coefficient of 0.9960, 0.9970, and 0.9997, respectively.

To further evaluate its feasibility and versatility as a platform toward microgravity biosensing, three routine physiological markers that are very close to astronaut's daily life include calcium (loss of bone calcium causing severe pain and decrease in bone density leading to bone fractures in microgravity), protein (helps to gain additional insight into protein changes that affect the human body due to microgravity), and glucose (the glucose level in serum, plasma, body fluid, food, and growth medium is a key diagnostic parameter for many metabolic disorders) were chose to illustrate the ability of performing biodetection. The nanodendritic superwettable microchips (superhydrophilic microwell diameter: 0.5 mm) were employed to perform the quantitatively colorimetrical detection of calcium, protein, and glucose (detailed detection processes are provided in the Experimental Section). As demonstrated in Figure 4, the reverse capture of microdroplets in the limited superhydrophilic microwells suggested its capturing capability against gravity. The visual detection of calcium, protein, and glucose can be achieved by observing color intensities of the welled microdroplets, which were recorded by using Lane 1D analysis software to read the grayscale value. The corresponding calibration plot of colorimetric intensities *vs* calcium, protein, and glucose concentrations was linear with correlation coefficients of 0.9960, 0.9970, and 0.9997, respectively, confirming its suitability for quantitative work. In addition, the reproducibility of the superwettable microchips was visually examined by two rows of same sample solutions; the observation of almost the same color intensity in contrast rows indicated its fine analytical reproducibility. Such superwettable microchips with the capability of capturing microdroplets against gravity provide unlimited possibilities in quantitative biosensing under a microgravity environment.

CONCLUSION

In conclusion, we introduced the superhydrophilic–superhydrophobic microchips as a biosensing platform, providing a simple, easy to operate, low-weight, and easy read-out technology to detect routine physiological markers toward microgravity applications. The nanodendritic structure in superhydrophilic microwells could generate capillary force and capture different volumes of microdroplets against the gravity by designing the diameters of superhydrophilic microwells. Capillary theoretical model on porous solid surfaces can explain the unique capability of superwettable microchips capturing water microdroplets against gravity. Such capability allows the superwettable microchip as biosensing platform in visual detection of routine physiological markers, such as calcium, protein, and glucose. This study shows promising applications toward biosensing in microgravity conditions and studying the influence of microgravity (such as cellular function, the immune system, the skeleton of laboratory animals, and expression of proteins) in the Space Station spaceflight laboratory.

EXPERIMENTAL SECTION

Preparation of Nanodendritic Silica Coatings. The nanodendritic silica substrate was fabricated according to previous literatures as follows: First, glass slides were cleaned by piranha solution (mixture of 3:1 (v/v) 98% H_2SO_4 and 30% H_2O_2) for 1 h, followed by ultrasonicating for 0.5 h in ethanol, acetone, and ultrapure water, respectively, and drying with nitrogen gas. Then, a layer of candle soot was deposited on the cleaned glass slide by moving the substrate back and forth on a steady burning candle at a constant speed seven times. Subsequently, the candle soot layer was coated with a silica shell by chemical vapor deposition (CVD) of TEOS at 30 °C using an ammonia solution as a catalyst in a desiccator for 36 h. Finally, the candle soot particles were removed by calcinating the carbon/silica core/shell nanocomposite at 550 °C for 2 h.

Fabrication of Superhydrophilic–Superhydrophobic Microwells. First, the nanodendritic silica coating was treated with oxygen plasma (DT-03, China) at 100 W for 180 s and then immersed in an anhydrous toluene (99.8%) solution containing 1 vol % octadecytrichlorosilane (OTS) for 1 h under a nitrogen gas atmosphere at room temperature. Then, the OTS-modified nanodendritic silica coating was rinsed with toluene, ethanol, and ultrapure water, respectively, and blown dry with nitrogen gas, followed by baking at 120 °C for 10 min. A high-pressure mercury lamp (at about 150 mW/cm^2) was used to irradiate the OTS-modified nanodendritic silica coating through a photomask for 40 min in ambient air. The nonirradiated part remained superhydrophobic; in contrast, the UV irradiated regions became superhydrophilic.

Detection of Calcium, Protein, and Glucose. The calcium content was colorimetrically determined by the *o*-cresolphthalein complexone method (Calcium Kit; Sigma-Aldrich). Two μL sodium acetate-ethylene diamine buffer (pH = 11) and 2 μL color reagent were added carefully to the microwells at room temperature, then 1 μL calcium ion standard solution with concentrations of 0, 0.4 (16 ng),

DOI: 10.1021/acsnano.6b06896
ACS Nano 2017, 11, 621–626

0.8, 1.2, 1.6, 2.0, 2.5, and 3.0 mM were carefully drop-cast onto the microwells, respectively. Finally, a camera was used to record the pictures, and the Lane 1D analysis software was used to read the grayscale value. Finally, the corresponding calibration plot of colorimetric intensities *vs* the target calcium ion was obtained, which was linear with a correlation coefficient of 0.9960. The concentration of BSA was colorimetrically determined by the interaction of Bromophenol Blue with proteins in acidic solution. Bromophenol Blue solution (pH = 3, citrate buffer, 3.3 mM) was prepared and was carefully added (2.5 μL) to the microwells at room temperature, then 2.5 μL BSA standard solution with concentrations of 0.1, 0.3, 0.5, 0.7, 0.9, 1.2, 1.5, and 2.0 mM was carefully drop-cast onto the microwells, respectively. By using the same approach as calcium, the finally linear calibration plot of colorimetric intensities *vs* the target concentration of BSA was obtained with a coefficient of 0.9970. Using the reaction of glucose oxidase (GOx) oxidation of glucose to produce hydrogen peroxide (H_2O_2), the generated color by H_2O_2 oxidation of potassium iodide (KI) is proportional to the glucose amount. Two μL KI (0.6M) and 2 μL GOx (15 U/mL) were added carefully to the microchips at room temperature, then 1 μL glucose solution with concentrations of 0, 2, 4, 6, 8, 10, 15, and 20 mM was drop-cast onto the microwells, respectively. By using the same approach as calcium, the finally linear calibration plot of colorimetric intensities *vs* the target concentration of glucose was obtained with a coefficient of 0.9996.

ASSOCIATED CONTENT

Supporting Information

The Supporting Information is available free of charge on the ACS Publications website at DOI: 10.1021/acsnano.6b06896.

Detailed materials and instruments and supporting figures (PDF)

AUTHOR INFORMATION

Corresponding Authors

*E-mail: xuliping@ustb.edu.cn.
*E-mail: zhangxueji@ustb.edu.cn.
*E-mail: stwang@mail.ipc.ac.cn.

ORCID

Shutao Wang: 0000-0002-2559-5181

Notes

The authors declare no competing financial interest.

ACKNOWLEDGMENTS

The work is supported by National Natural Science Foundation of China (NSFC Grant no. 21475009, 21475008, 21275017), the Fundamental Research Funds for the Central Universities (FRF-TP-15-014A3), MOST (2013YQ190467), the Top-Notch Young Talents Program of China, and Beijing Municipal Science & Technology Commission (Z161100000116037).

REFERENCES

(1) Zayzafoon, M.; Meyers, V. E.; McDonald, J. M. Microgravity: the Immune Response and Bone. *Immunol. Rev.* **2005**, *208*, 267−280.

(2) DiFrancesco, J. M.; Olson, J. M. The Economics of Microgravity Research. *npj Microgravity* **2015**, *1*, 15001.

(3) Carmeliet, G.; Nys, G.; Stockmans, I.; Bouillon, R. Gene Expression Related to the Differentiation of Osteoblastic Cells is Altered by Microgravity. *Bone* **1998**, *22*, 139S−143S.

(4) Vico, L.; Collet, P.; Guignandon, A.; Lafage-Proust, M.-H.; Thomas, T.; Rehailia, M.; Alexandre, C. Effects of Long-Term Microgravity Exposure on Cancellous and Cortical Weight-Bearing Bones of Cosmonauts. *Lancet* **2000**, *355*, 1607−1611.

(5) Luna, C.; Yew, A. G.; Hsieh, A. H. Effects of Angular Frequency During Clinorotation on Mesenchymal Stem Cell Morphology and Migration. *npj Microgravity* **2015**, *1*, 15007.

(6) Higashibata, A.; Hashizume, T.; Nemoto, K.; Higashitani, N.; Etheridge, T.; Mori, C.; Harada, S.; Sugimoto, T.; Szewczyk, N. J.; Baba, S. A.; et al. Microgravity Elicits Reproducible Alterations in Cytoskeletal and Metabolic Gene and Protein Expression in Space-Flown Caenorhabditis Elegans. *npj Microgravity* **2016**, *2*, 15022.

(7) Tamma, R.; Colaianni, G.; Camerino, C.; Di Benedetto, A.; Greco, G.; Strippoli, M.; Vergari, R.; Grano, A.; Mancini, L.; Mori, G.; et al. Microgravity During Spaceflight Directly Affects *in vitro* Osteoclastogenesis and Bone Resorption. *FASEB J.* **2009**, *23*, 2549−2554.

(8) Jin, D. Q.; Zhu, Y.; Fang, Q. Swan probe: A nanoliter-scale and high-throughput sampling interface for coupling electrospray ionization mass spectrometry with microfluidic droplet array and multiwell plate. *Anal. Chem.* **2014**, *86*, 10796−10803.

(9) Yu, J.; Zhou, J.; Sutherland, A.; Wei, W.; Shin, Y. S.; Xue, M.; Heath, J. R. Microfluidics-Based Single-Cell Functional Proteomics for Fundamental and Applied Biomedical Applications. *Annu. Rev. Anal. Chem.* **2014**, *7*, 275−295.

(10) Tonooka, T.; Sato, K.; Osaki, T.; Kawano, R.; Takeuchi, S. Lipid Bilayers on A Picoliter Microdroplet Array for Rapid Fluorescence Detection of Membrane Transport. *Small* **2014**, *10*, 3275−3282.

(11) Xu, K.; Wang, X.; Ford, R. M.; Landers, J. P. Self-Partitioned Droplet Array on Laser-Patterned Superhydrophilic Glass Surface for Wall-less Cell Arrays. *Anal. Chem.* **2016**, *88*, 2652−2658.

(12) Hansen, M. M.; Meijer, L. H.; Spruijt, E.; Maas, R. J.; Rosquelles, M. V.; Groen, J.; Heus, H. A.; Huck, W. T. Macromolecular Crowding Creates Heterogeneous Environments of Gene Expression in Picolitre Droplets. *Nat. Nanotechnol.* **2016**, *11*, 191−197.

(13) Balu, B.; Berry, A. D.; Hess, D. W.; Breedveld, V. Patterning of Superhydrophobic Paper to Control the Mobility of Micro-Liter Drops for Two-Dimensional Lab-On-Paper Applications. *Lab Chip* **2009**, *9*, 3066−3075.

(14) Kobayashi, T.; Shimizu, K.; Kaizuma, Y.; Konishi, S. Novel Combination of Hydrophilic/Hydrophobic Surface for Large Wettability Difference and Its Application To Liquid Manipulation. *Lab Chip* **2011**, *11*, 639−644.

(15) Cao, M.; Li, K.; Dong, Z.; Yu, C.; Yang, S.; Song, C.; Liu, K.; Jiang, L. Superhydrophobic "Pump": Continuous and Spontaneous Antigravity Water Delivery. *Adv. Funct. Mater.* **2015**, *25*, 4114−4119.

(16) Seo, J.; Lee, S. K.; Lee, J.; Seung Lee, J.; Kwon, H.; Cho, S. W.; Ahn, J. H.; Lee, T. Path-Programmable Water Droplet Manipulations on An Adhesion Controlled Superhydrophobic Surface. *Sci. Rep.* **2015**, *5*, 12326.

(17) Gu, Z. Z.; Fujishima, A.; Sato, O. Patterning of A Colloidal Crystal Film on A Modified Hydrophilic and Hydrophobic Surface. *Angew. Chem., Int. Ed.* **2002**, *41*, 2067−2070.

(18) Zhang, X.; Jin, M.; Liu, Z.; Tryk, D. A.; Nishimoto, S.; Murakami, T.; Fujishima, A. Superhydrophobic TiO_2 Surfaces: Preparation, Photocatalytic Wettability Conversion, and Superhydrophobic-Superhydrophilic Patterning. *J. Phys. Chem. C* **2007**, *111*, 14521−14529.

(19) Nishimoto, S.; Sekine, H.; Zhang, X.; Liu, Z.; Nakata, K.; Murakami, T.; Koide, Y.; Fujishima, A. Assembly Of Self-Assembled Monolayer-Coated Al_2O_3 on Tio_2 Thin Films for the Fabrication of Renewable Superhydrophobic-Superhydrophilic Structures. *Langmuir* **2009**, *25*, 7226−7228.

(20) Oliveira, N. M.; Reis, R. L.; Mano, J. F. Superhydrophobic Surfaces Engineered Using Diatomaceous Earth. *ACS Appl. Mater. Interfaces* **2013**, *5*, 4202−4208.

(21) Neto, A. I.; Demir, K.; Popova, A. A.; Oliveira, M. B.; Mano, J. F.; Levkin, P. A. Fabrication of Hydrogel Particles of Defined Shapes Using Superhydrophobic-Hydrophilic Micropatterns. *Adv. Mater.* **2016**, *28*, 7613−7619.

(22) Xu, L. P.; Chen, Y.; Yang, G.; Shi, W.; Dai, B.; Li, G.; Cao, Y.; Wen, Y.; Zhang, X.; Wang, S. Ultratrace DNA Detection Based on the Condensing-Enrichment Effect of Superwettable Microchips. *Adv. Mater.* **2015**, *27*, 6878−6884.

(23) Ueda, E.; Levkin, P. A. Emerging Applications of Superhydrophilic-Superhydrophobic Micropatterns. *Adv. Mater.* **2013**, *25*, 1234−1247.
(24) Feng, W.; Li, L.; Ueda, E.; Li, J.; Heißler, S.; Welle, A.; Trapp, O.; Levkin, P. A. Surface Patterning *via* Thiol-Yne Click Chemistry: An Extremely Fast and Versatile Approach to Superhydrophilic-Superhydrophobic Micropatterns. *Adv. Mater. Interfaces* **2014**, *1*, 1400269.
(25) Oliveira, M. B.; Neto, A. I.; Correia, C. R.; Rial-Hermida, M. I.; Alvarez-Lorenzo, C.; Mano, J. F. Superhydrophobic Chips for Cell Spheroids High-Throughput Generation and Drug Screening. *ACS Appl. Mater. Interfaces* **2014**, *6*, 9488−9495.
(26) Popova, A. A.; Schillo, S. M.; Demir, K.; Ueda, E.; Nesterov-Mueller, A.; Levkin, P. A. Droplet-Array (DA) Sandwich Chip: A Versatile Platform for High-Throughput Cell Screening Based on Superhydrophobic-Superhydrophilic Micropatterning. *Adv. Mater.* **2015**, *27*, 5217−5222.
(27) Li, H.; Yang, Q.; Li, G.; Li, M.; Wang, S.; Song, Y. Splitting A Droplet for Femtoliter Liquid Patterns and Single Cell Isolation. *ACS Appl. Mater. Interfaces* **2015**, *7*, 9060−9065.
(28) Shi, F.; Niu, J.; Liu, J.; Liu, F.; Wang, Z.; Feng, X. Q.; Zhang, X. Towards Understanding Why a Superhydrophobic Coating Is Needed by Water Striders. *Adv. Mater.* **2007**, *19*, 2257−2261.
(29) Krumpfer, J. W.; McCarthy, T. J. Dip-Coating Crystallization on A Superhydrophobic Surface: A Million Mounted Crystals in A 1 Cm2 Array. *J. Am. Chem. Soc.* **2011**, *133*, 5764−5766.
(30) Tian, D.; Song, Y.; Jiang, L. Patterning of Controllable Surface Wettability for Printing Techniques. *Chem. Soc. Rev.* **2013**, *42*, 5184−5209.
(31) Liu, H.; Liu, X.; Meng, J.; Zhang, P.; Yang, G.; Su, B.; Sun, K.; Chen, L.; Han, D.; Wang, S.; Jiang, L. Hydrophobic Interaction-Mediated Capture and Release of Cancer Cells on Thermoresponsive Nanostructured Surfaces. *Adv. Mater.* **2013**, *25*, 922−927.
(32) Celia, E.; Darmanin, T.; Taffin de Givenchy, E.; Amigoni, S.; Guittard, F. Recent Advances in Designing Superhydrophobic Surfaces. *J. Colloid Interface Sci.* **2013**, *402*, 1−18.
(33) Wang, S.; Liu, K.; Yao, X.; Jiang, L. Bioinspired Surfaces with Superwettability: New Insight on Theory, Design, and Applications. *Chem. Rev.* **2015**, *115*, 8230−8293.
(34) Gauthier, A.; Symon, S.; Clanet, C.; Quere, D. Water Impacting on Superhydrophobic Macrotextures. *Nat. Commun.* **2015**, *6*, 8001.
(35) Kreder, M. J.; Alvarenga, J.; Kim, P.; Aizenberg, J. Design of Anti-Icing Surfaces: Smooth, Textured Or Slippery? *Nat. Rev. Mater.* **2016**, *1*, 15003.
(36) Su, B.; Tian, Y.; Jiang, L. Bioinspired Interfaces with Superwettability: From Materials to Chemistry. *J. Am. Chem. Soc.* **2016**, *138*, 1727−1748.
(37) Liu, C.; Ju, J.; Zheng, Y.; Jiang, L. Asymmetric Ratchet Effect for Directional Transport of Fog Drops on Static and Dynamic Butterfly Wings. *ACS Nano* **2014**, *8*, 1321−1329.
(38) Zhang, P.; Liu, H.; Meng, J.; Yang, G.; Liu, X.; Wang, S.; Jiang, L. Grooved Organogel Surfaces Towards Anisotropic Sliding of Water Droplets. *Adv. Mater.* **2014**, *26*, 3131−3135.
(39) Zhang, M.; Wang, L.; Hou, Y.; Shi, W.; Feng, S.; Zheng, Y. Controlled Smart Anisotropic Unidirectional Spreading of Droplet on a Fibrous Surface. *Adv. Mater.* **2015**, *27*, 5057−5062.
(40) Jin, M.; Feng, X.; Feng, L.; Sun, T.; Zhai, J.; Li, T.; Jiang, L. Superhydrophobic Aligned Polystyrene Nanotube Films with High Adhesive Force. *Adv. Mater.* **2005**, *17*, 1977−1981.
(41) Wu, D.; Wu, S. Z.; Chen, Q. D.; Zhang, Y. L.; Yao, J.; Yao, X.; Niu, L. G.; Wang, J. N.; Jiang, L.; Sun, H. B. Curvature-Driven Reversible *In Situ* Switching Between Pinned and Roll-Down Superhydrophobic States for Water Droplet Transportation. *Adv. Mater.* **2011**, *23*, 545−549.
(42) Fobel, R.; Kirby, A. E.; Ng, A. H.; Farnood, R. R.; Wheeler, A. R. Paper Microfluidics Goes Digital. *Adv. Mater.* **2014**, *26*, 2838−2843.
(43) Whitesides, G. M. The Origins and the Future of Microfluidics. *Nature* **2006**, *442*, 368−373.
(44) Posthuma-Trumpie, G. A.; Korf, J.; van Amerongen, A. Lateral Flow (Immuno) Assay: Its Strengths, Weaknesses, Opportunities and Threats. A Literature Survey. *Anal. Bioanal. Chem.* **2009**, *393*, 569−582.
(45) Köylü, Ü. Ö.; Faeth, G. M.; Farias, T. L.; Carvalho, M. G. Fractal and Projected Structure Properties of Soot Aggregates. *Combust. Flame* **1995**, *100*, 621−633.
(46) Deng, X.; Mammen, L.; Butt, H.-J.; Vollmer, D. Candle Soot as a Template for a Transparent Robust Superamphiphobic Coating. *Science* **2012**, *335*, 67−70.
(47) Yang, G.; Liu, H.; Liu, X.; Zhang, P.; Huang, C.; Xu, T.; Jiang, L.; Wang, S. Underwater-Transparent Nanodendritic Coatings for Directly Monitoring Cancer Cells. *Adv. Healthcare Mater.* **2014**, *3*, 332−337.
(48) Denesuk, M.; Smith, G. L.; Zelinski, B. J. J.; Kreidl, N. J.; Uhlmann, D. R. Capillary Penetration of Liquid Droplets into Porous Materials. *J. Colloid Interface Sci.* **1993**, *158*, 114−120.
(49) Bikerman, J. J. *The Science of Adhesive Joints*, 2nd ed.; Academic Press: New York, 1968.

DOI: 10.1021/acsnano.6b06896
ACS Nano 2017, 11, 621−626